

# Interface Tracking of Accreting Ice on a Wind Turbine Airfoil or a Cable due to Impinging Droplets

M. Milanez and M. Farzaneh

*NSERC/Hydro-Quebec/UQAC Industrial Chair on Atmospheric Icing of Power, Network Equipment (CIGELE) and Canada Research Chair on Engineering of Power, Network Atmospheric Icing (INGIVRE), University of Quebec at Chicoutimi, Quebec, Canada G7H 2B1*  
[www.cigele.ca](http://www.cigele.ca)

**Abstract**—In order to assess damage caused by icing to power network equipment in cold climate regions, the characteristics of local ice growth need to be determined. For this purpose, a simple icing model is developed based on droplet motion with air under supercooled atmospheric conditions. A laminar two-phase flow is assumed to impact the ice-prone surfaces during ice deposition. In the flow part of the domain, a 'two fluid' model of droplet flow and air is adopted. Drag, gravity and buoyancy externally control droplet motion in this low droplet phase fraction investigation. The leading edge boundary of the accumulating ice bulk moves toward the impinging flow. The parametric study encompasses illustrative simulations of dry ice accretion on open surfaces involving predictions of the evolving interfaces from an airfoil and a cable. The proposed model offers practical estimations of the morphology of accreted ice on the equipment. Icing caused degradation of aerodynamic and structural performances can be evaluated from these studies. The model may also be used for further comparative and validation efforts of other models and parametric studies in sub/supercooled icing conditions.

## I. INTRODUCTION

ICING of power network equipment surfaces (PNES) degrades performance of the equipment. Modeling and analysis of freezing and impinging flows on PNES can lead to minimization/maximization of undesired/desired effects on the equipment. Onset of icing usually depends on presence of moving droplets, interacting with air and exposed surfaces, such as wind turbine blades and cables. Ice growth and propagation of ice interface are also controlled by degree of diluteness of dispersed droplet flow in the air. An evolving ice area with its mass increasingly hinders a performance of the equipment. To understand icing of such structures, closer theoretical and experimental studies are needed. Motivation for the present paper is to uncover basic relations of icing processes on PNES by a simple Lagrangian model and using it in the future with a more comprehensive model for icing of PNES.

Researchers have modeled multiphase flows with droplets, leading to icing of airfoils or cables in a variety of ways. While engineering Eulerian [1]-[3] framework is more suitable for tracking a group of droplets and solving its velocity field, the Lagrangian [4] one is more apt to track a single particle (droplet) and solve its trajectory. Bragg mainly studied icing of aircraft airfoils and its influences on their aerodynamic performances [5]. He also studied icing effects on a wind

turbine and a performance of the turbine with Jasinski [6]-[7]. Among the pioneers of modeling and studies of wind turbine icing, Finstad and Makkonen [8] are noteworthy. Their work was extended to include potential flow calculations at low speeds and high impact angles and ice density [9]. Makkonen and co-workers extended the model to include wet ice growth [10]. Icing of power equipment was studied for a range of applications including transmission lines with physical (Goodwin [11]) and electrical (Farzaneh [12], [13]) loads on conductors and insulators. Makkonen modeled ice accretion on wires [14] and a rough cylinder [15].

The proposed Lagrangian model includes determination of disperse droplet motion in continuous air, droplet impingement characteristics on PNES with freezing and icing of PNES. Interfacial two-phase drag, gravity and buoyancy externally control the motion of a discrete spherical droplet, modeled as a particle. Empirical drag coefficients are determined by means of [16]. The ice tracking is added to initial Lagrangian discrete phase framework. Three moving phases and one stationary phase in contact resemble icing of a wind turbine with NACA 63-212 airfoil and a cable. Illustrative cases involve situations with co-existing and (re)joining flows as they set off the onset for dry icing. Ice interfaces are investigated mainly under no-drag and drag conditions with different droplet and air velocity, different droplet phase fraction and icing times. These simplistic solutions can be useful for comparison with the results of other models and parametric study for e. g. determination of transport properties. Future adaptation will incorporate air equations with phase pressure fields and study of an aerodynamic performance of power network equipment.

## II. ICING MODELING

Icing involves modeling of liquid (water droplet-d) and gas (air-a) flows, impact and freezing of droplets on PNES and ice evolution from PNES into a flow domain. The modeling is based on a Lagrangian point force framework for a discrete droplet phase. Solutions of acceleration, velocity and trajectory for the droplet transport with air can be calculated from balances of the inertia with interfacial drag, gravity and buoyancy. Physical model of the multiphase droplet traveling through the air can be described by the following two dimensional transport equations in/for a flow domain:

$$\zeta_i \frac{dv_{d,x}}{dt} = -\zeta_d |\vec{v}_d - \vec{v}_a| (v_{d,x} - v_{a,x}), \quad (1)$$

$$\zeta_i \frac{dv_{d,y}}{dt} = -\zeta_d |\vec{v}_d - \vec{v}_a| (v_{d,y} - v_{a,y}) + (\zeta_g - \zeta_b)g, \quad (2)$$

$$\frac{d}{dt}(\beta_d \rho_d) = 0, \quad (3)$$

where mass related coefficients are expressed as  $\zeta_i = \rho_d \pi D_d^3 / 6$ ,  $\zeta_d = (\rho_a / 2) C_D \pi D_d^2 / 4$ ,  $\zeta_g = \rho_d g \pi D_d^3 / 6$  and  $\zeta_b = \rho_a g \pi D_d^3 / 6$ . Symbols  $v$ ,  $t$ ,  $g$ ,  $\rho$ ,  $D$  and  $C_D$  represent a velocity magnitude, flowing time, a gravity constant, specific density, a diameter (regarded as median volume diameter MVD) and a drag coefficient, respectively. The drag coefficient can be estimated for a range of relative Reynolds numbers by the following expression

$$C_D = \frac{c_1}{Re_r^2} + \frac{c_2}{Re_r} + c_3, \quad (4)$$

where coefficients are defined in [16]. The Reynolds number between phases in contact in each direction,  $Re_r$ , is defined for a droplet phase as  $Re_r = \rho_a |\vec{v}_d - \vec{v}_a| D_d / \mu_a$ , where  $\mu$  represents a dynamic viscosity. In addition to a typical discrete flow system (1)-(2), degenerative form (3) ( $\Rightarrow \beta_d = \text{const.}$ ,  $\beta_d = \beta_{d,IN}$ ) of an equation for dispersed phase fraction from the Eulerian approach is adopted in the flow domain for use in the subsequent icing modeling. In conventional Lagrangian tracking,  $\beta_d$  can be assumed very small (neglected). In this study,  $\beta_d$  is assumed to be small enough to neglect droplet-droplet interactions, while it is used in the icing modeling.

Fig. 1 sketches a physical domain with PNES, e.g. an airfoil or a cable. Boundary conditions for the quantities of the phases are at their inlets of a Diriclet type. Boundary conditions at all other locations are of a Neumann (natural) type. The procedure developed is used to investigate ice accretion on PNES by horizontally and vertically emitting droplets and air into the domain. The study involves the characterization of evolution of ice interface as it relates to the initial droplet and air velocity, a droplet diameter and droplet phase fraction. The study is carried out with a variety of water/droplet and air properties. The presented results include properties at freezing conditions  $T = 0^\circ C$ .

### III. ICE TRACKING

The ice tracking accompanies the flow part of the modeling. Droplets impinge on an arbitrary surface of PNES (e.g. airfoil or cable). Impinging positions are determined also based on the air phase. Upon impact at their full velocity, the impinging droplets change their phase instantaneously (freeze) and adhere to the surface. The mass of the impinged water droplets equals that of the resulting accreted dry ice. This ice mass is forming the two-dimensional stationary ice/PNES and moving ice/flow interfaces at its boundaries. The accreted ice gradually occupies more space in front of PNES. Flow conditions are continuously updated at the moving interface

with the same conditions as those when the flows impacted PNES surfaces. The velocity of the accreting ice is also controlled by the droplet phase fraction.

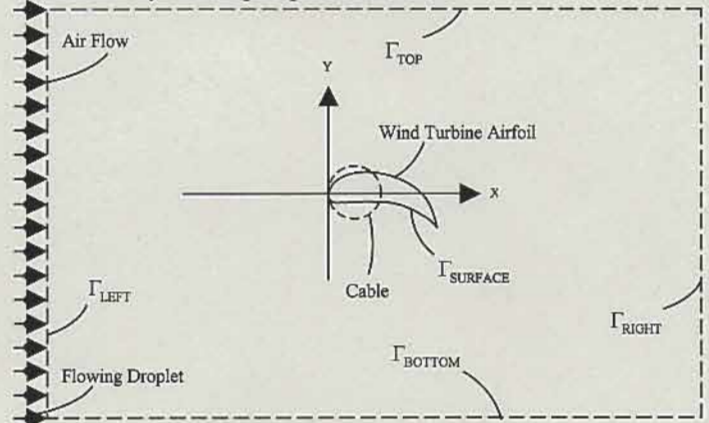


Fig. 1. Schematics of a problem.

Ice interface simulations are carried out under various conditions. A general solution for the ice interface can be expressed as follows:

$$f(x_{i,j}, \lambda_{j,k}, \Delta t_{ICE}) = \begin{cases} \chi(x_{i,U}, \lambda_{U,k}, \Delta t_{ICE}), & \chi_0 \leq \chi \\ \varepsilon(x_{i,D}, \lambda_{D,k}, \Delta t_{ICE}), & \varepsilon_0 > \varepsilon \end{cases} \quad (5)$$

As an illustrative function of/over x-direction for approximating ice interface and PNES profiles, let us consider  $f(x, \lambda_{j,k}, t_{ICE}) =$

$$\lambda_{i,1}x^6 + \lambda_{i,2}x^5 + \lambda_{i,3}x^4 + \lambda_{i,4}x^3 + \lambda_{i,5}x^2 + \lambda_{i,6}x + \lambda_{i,7}, \quad (6)$$

where symbols  $i$  and  $\Delta t_{ICE}$  identify direction and time duration of ice growth, respectively. For example, the ice interface simulation for Case AD1, which is presented in Section IV (Icing Simulations) is used here. Table I contains the data for the interface at  $\Delta t_{ICE} = 30$  s and  $\beta_{d,IN} = 5 \cdot 10^{-4}$ , and the profile of the airfoil. Symbols  $\chi_0 = 0$  and  $\varepsilon_0 = 0$  represent locations from which the interfaces are approximated.

TABLE I  
COMPARISONS OF ICE THICKNESSES

T=30 s	$\lambda_{j,1}$	$\lambda_{j,2}$	$\lambda_{j,3}$	$\lambda_{j,4}$	$\lambda_{j,5}$	$\lambda_{j,6}$	$\lambda_{j,7}$
$\chi_0 \leq \chi$							
$\varepsilon_0 > \varepsilon$							
$5 \cdot 10^{-4}$	0.000	0.000	0.000	4.731	-1.821	0.261	0.046
	0.000	0.000	10.098	-5.811	1.366	-0.194	-0.040
NACA	-3.043	10.066	12.818	8.087	-2.925	0.626	0.007
63-212	2.324	-7.888	10.194	-6.499	2.359	-0.483	-0.006

For a one-dimensional or quasi two-dimensional growing ice-interface (though ice occupies two dimensions, it grows solely in one direction) ice thickness can be calculated from

$$\Delta h_{ICE} = \beta_{d,IN} v_d \Delta t_{ICE}, \quad \Delta t_{ICE} = t - t_{IMP}. \quad (7)$$

Variable  $\Delta h_{ICE}$  identifies ice growth. Both  $\Delta h_{ICE}$  and  $\Delta t_{ICE}$  values are considered from an instant of the flow impact on PNES ( $t_{IMP}$ ), during ice accretion. An arbitrary area occupied by ice, existing between its interfaces can be fully determined along all principal directions as:

$$\begin{aligned}
 A_{ICE} = & \int_{A_x} [\chi(x_U, \lambda_U, \Delta t_{ICE}) - \varepsilon(x_U, \lambda_U, \Delta t_{ICE})] dA \\
 & + \int_{A_x} [\chi(x_D, \lambda_D, \Delta t_{ICE}) - \varepsilon(x_D, \lambda_D, \Delta t_{ICE})] dA \\
 & + \int_{A_y} [\chi(y_U, \lambda_U, \Delta t_{ICE}) - \varepsilon(y_U, \lambda_U, \Delta t_{ICE})] dA \\
 & + \int_{A_y} [\chi(y_D, \lambda_D, \Delta t_{ICE}) - \varepsilon(y_D, \lambda_D, \Delta t_{ICE})] dA.
 \end{aligned} \quad (8)$$

By knowing the limits of integration for a particular case the ice area can be calculated from (8).

The mass of ice in a unit ice region (2D case) is given by

$$m_{ICE} = \rho_{ICE} A_{ICE}, \quad (9)$$

while that of quasi 2D ice is

$$m_{ICE} = \rho_{ICE} \Delta h_{ICE} A_{ICE}. \quad (10)$$

#### IV. ICING SIMULATIONS

Dry ice simulations are carried out based on droplet and air flows impacting the airfoil or a cylindrical cable in various conditions. Ice interface evolution is analyzed with respect to interfacial drag conditions (none, weak and strong) involving various inlet droplet and air velocities, droplet size and phase fractions. The ice (interface) spread is presented at icing times in the icing figures, such as:  $\Delta t_{ICE}$  (s) = 0, 30, 60, 90 and 120.

Time duration  $\Delta t_{ICE} = 0$  s corresponds to the beginning of ice accretion on the airfoil or cable surface. The ice interface is presented by the series of dots along the particular section of the surface. The ice interface evolution in the figures is shown at time step 30 s from the surface. The last (fourth) drawn ice interface in the figures, counted from (excluding) the surface corresponds to ice interface time 120 s.

##### A. Ice accretion on an airfoil

The airfoil used in this study is of NACA 63-212 type. Its geometry is presented in relevant figures below.

###### 1) No-drag formulation based analysis

The first case, AD01, is presented in Fig. 2. It considers horizontally emitted droplet flow at boundary  $\Gamma_{LEFT}$  into a computational domain. Its inlet velocity is  $[v_{d,x,0}, v_{d,y,0}] = [5.0, 0.0]$  m/s. The selected speed is high enough to reach nearly horizontal flow for a distance of 1.2 m, thus allowing investigation of ice accretion in a unidirectional manner. The droplet phase fraction is  $\beta_d = 0.0001$ . The droplets impact the surface at their full velocity  $[(\partial \bar{v}_d / \partial \bar{n})_w = 0]$ . The other droplets, which do not reach the surface of the airfoil pass it in a nearly horizontal direction. Air is exempt from this simulation.

A resultant shape of the simulated ice interface roughly imitates the leading edge of the airfoil profile (similar shapes). The ice profile is not symmetrical, which is expected. A quantified analysis of the ice interface propagation is conducted based on a leftward moving leading tip of the interface. The ice thickness is calculated based on (7) and

compared with the corresponding computed values as shown in Table II. The speed of the interface propagation is calculated from the expression,  $v_{d,ICE} = \Delta h_{ICE} / \Delta t_{ICE}$ . The percentage difference of the ice thickness between the two cases is calculated by the following expression

$$\%DIFF = 100 (\Delta h_{ICE, x, comp} - \Delta h_{ICE}) / \Delta h_{ICE}. \quad (11)$$

A good agreement between these two sets of values is presented in Table II.

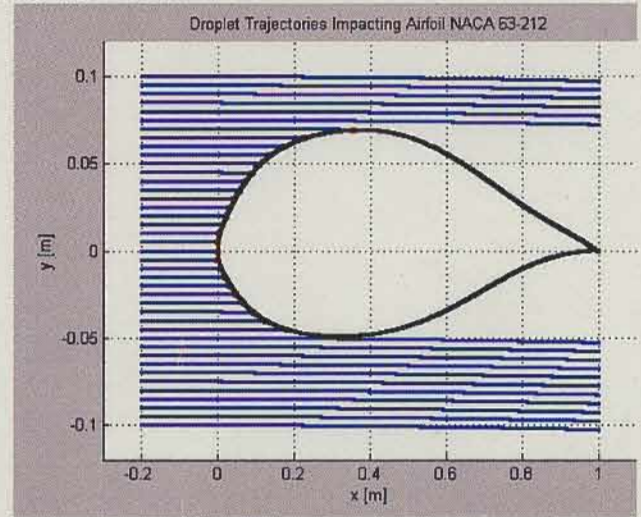


Fig. 2. Case AD01.

TABLE II  
COMPARISONS OF ICE THICKNESS

$\Delta t$ (s)	$\Delta h_{ICE, x, comp}$ (m)	$\Delta h_{ICE}$ (m)	%DIFF
0.0	0.00	0.00	0.0
30.0	0.15	0.15	0.0
60.0	0.30	0.30	0.0
90.0	0.45	0.45	0.0
120.0	0.60	0.60	0.0

The second case, AD02, depicted in Fig. 3 occurs when the droplet flow is horizontally emitted in an empty computational domain at boundary  $\Gamma_{LEFT}$ . Its inlet velocity is  $[v_{d,x,0}, v_{d,y,0}] = [5.0, 0.0]$  m/s. Due to zero drag, the droplet flow turns downward soon, which can also be observed from the ice shape and its evolution in the figure. It can be noticed that ice accretes faster on the upper portion of the impacted section of the airfoil than on the lower portion. This is mainly due to the fact that there is a larger normal component of droplet velocity on the upper surface of the airfoil than on the lower one. Similarly to the other cases, there is no droplet-air 'carving' of accreting ice nor a resultant groove at the stagnation locations. This is viewed to be mainly due to the exclusion of pressure from the simulations.

###### 2) Drag formulation based analysis

➤ In the first case, Case AD1, the droplet flow is assumed to enter the computational domain from boundary  $\Gamma_{LEFT}$  (Fig. 1), while air enters the domain at boundary  $\Gamma_{BOTTOM}$ . The initial droplet velocity is  $[v_{d,x,0}, v_{d,y,0}] = [5.0, 0.0]$  m/s. The initial air velocity is  $[v_{a,x,0}, v_{a,y,0}] = [0.0, 3.0]$  m/s. Influence of droplet phase fraction on ice accretion and interface evolution

from the airfoil is presented. The shapes of ice interfaces are different in this case than in case AD01 due to the air influence on droplets and different phase fraction.

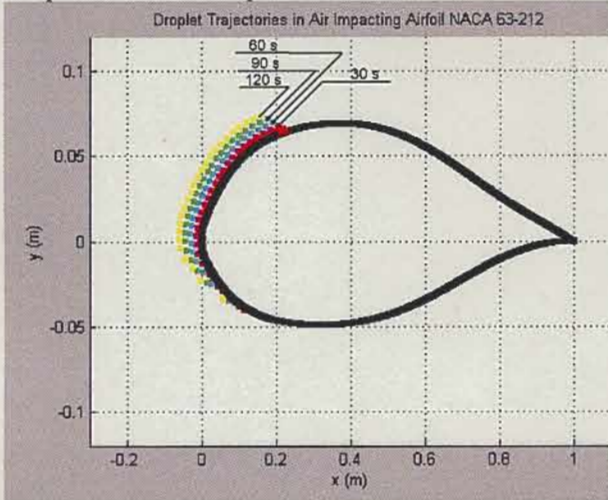


Fig. 3. Icing: Case AD02 (ice interface time step is 30 s).

In example AD1a (Fig. 4), a simulation with droplet phase fraction of  $\beta_d = 0.00005$  is carried out. Slower ice growth with smaller ice thickness with respect to the second example in Fig. 5 can be observed. This is expected as the phase fraction in this case is two times smaller than in AD1b.

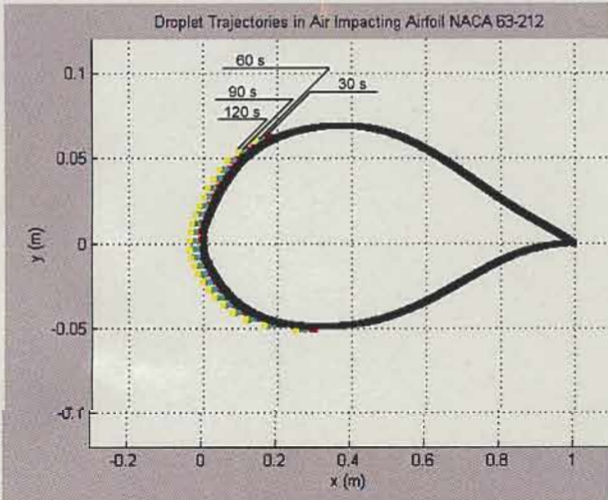


Fig. 4. Icing: Case AD1a (ice interface time step is 30 s).

The second example, presented in Fig. 5 shows a simulation with droplet phase fraction  $\beta_d = 0.0001$ . It can be noted that less/more ice accretes on the upper/lower surface of the airfoil than in Case AD02 due to the droplet flow being deflected upward by the air flow.

Simulations with  $\beta_d > 0.00005$  yield larger ice thickness at the same times as for Case AD1, which is expected. Fig. 6 presents the horizontal distance reached (x-absolute coordinate) by the two most distant locations of the particular interface (its lower and upper sides/edges) as a function of droplet phase fraction. Ice accretes at the larger, approx. linear rate at the upper side than the lower side of the interface with increasing phase fraction. This trend is observed at all times. For example, using pressure formulation in air equations may

generally alter the accretion rate along entire ice interface from approximately linear to nonlinear. The local pressure would additionally affect the evolving shape of the ice interface.

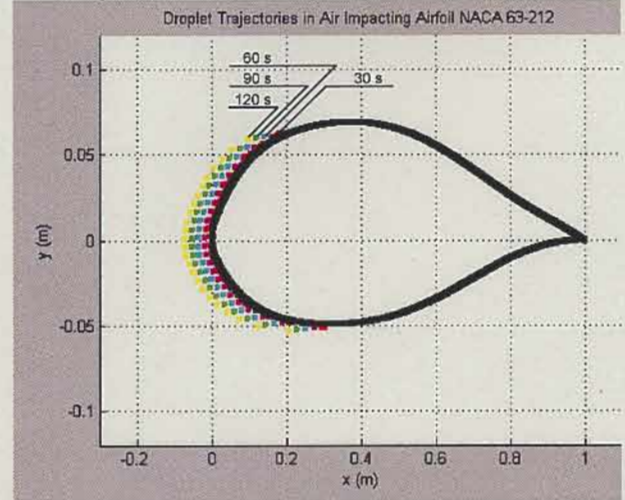


Fig. 5. Icing: Case AD1b (ice interface time step is 30 s).

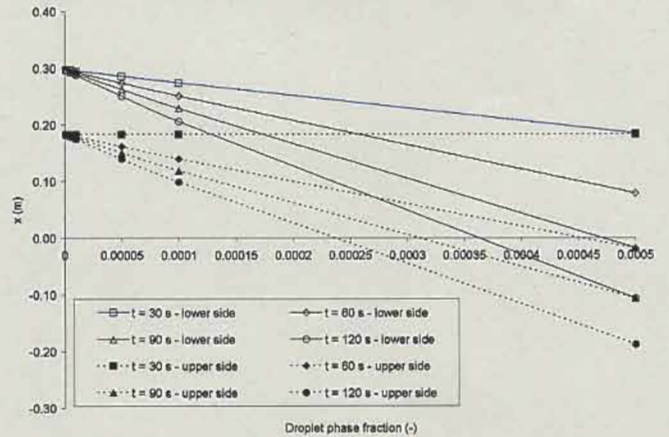


Fig. 6. Case AD1b: lower and upper edges of the accreted ice.

Fig. 7 compares examples of ice accretion on the airfoil at time  $t = 60$  s. A various values of droplet phase fraction from  $\beta_d = 0.000005$  to  $\beta_d = 0.0005$  are used. It can be noticed that ice accretion is fastest for the case with the largest fraction. Less/more ice accretes on the upper/lower surface of the airfoil than in Case AD02 due to the droplet flow being deflected upward by the air.

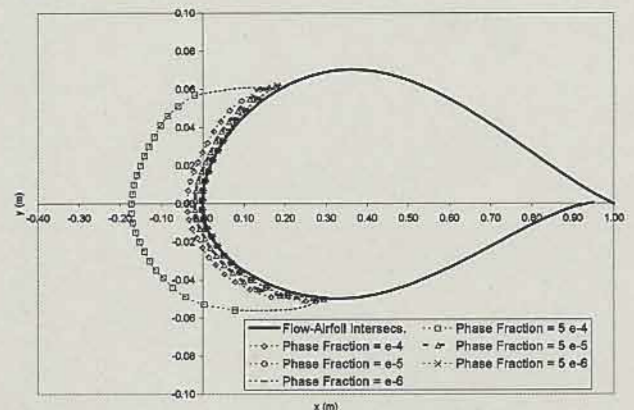


Fig. 7. Cases of icing on the airfoil with different  $\beta_d$  values.

Fig. 8 presents a rate of ice interface evolution (selected upper and lower edges) as a function of droplet phase fraction. The approximately linear rate is slightly larger at the upper than at the lower side due to the asymmetrical impingement of the flow on the airfoil. This phenomenon can be observed at all icing times.

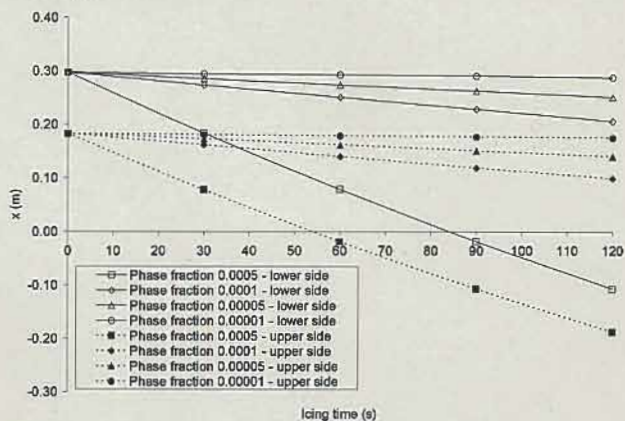


Fig. 8. Case AD1b: lower and upper edges of the accreted ice.

➤ In the second case, Case AD2, the droplet flow enters the computational domain from its top at  $\Gamma_{TOP}$ . Air enters the domain at boundary  $\Gamma_{LEFT}$ , ( $\perp$  to droplet flow). Simulations are performed with  $\beta_d = 0.0001$ . The influence of droplet and air velocities on ice accretion and ice interface evolution on the airfoil is presented.

First example AD2a in Fig. 9 considers the initial droplet and air velocity being  $[v_{d,x,0}, v_{d,y,0}] = [0.0, -2.0]$  m/s and  $[v_{a,x,0}, v_{a,y,0}] = [0.0, 0.0]$  m/s, respectively. Droplets move downward and impact only the upper surface of the airfoil. The smaller the scalar product of the droplet velocity vector and the normal to the airfoil surface is, the smaller is the ice thickness.

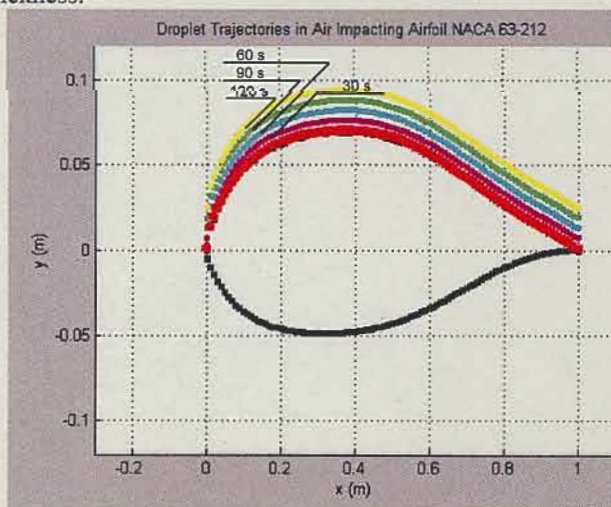


Fig. 9. Icing: Case AD2a (ice interface time step is 30 s).

In the second example, AD2b, shown in Fig. 10, the initial droplet and air velocity is considered to be  $[v_{d,x,0}, v_{d,y,0}] = [0.0, -2.0]$  m/s and  $[v_{a,x,0}, v_{a,y,0}] = [10.0, 0.0]$

m/s, respectively. The air flow hits the vertically streaming droplet flow and drags it toward the airfoil. At the same time, the air deflects the droplet flow rightward. Some droplet trajectories which start at x locations well before the tip (e. g. -0.2 m) of the airfoil are pushed against the airfoil with quite large curvature. This can be also seen on the shape of accreted ice at the tip.

### B. Ice accretion on a cable

A cylindrical cable of 0.05 m diameter is used in this simulation. Its center is shifted rightward to location  $[x_{c_0}, y_{c_0}] = [0.05, 0.00]$  m. Droplet phase fraction  $\beta_d = 0.00005$  is considered. The analysis of trajectories shows that the no-drag simulations given as examples, which are independent of a droplet diameter correspond to the drag-based ones with a droplet diameter of at least  $D_d = 0.005$  m.

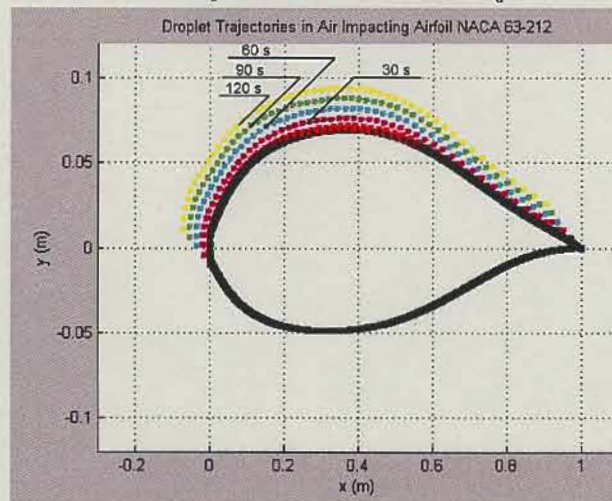


Fig. 10. Icing: Case AD2b (ice interface time step is 30 s).

#### 1) No-drag formulation based analysis

The first case, CD01, presented in Fig. 11, considers horizontally emitted droplet flow at boundary  $\Gamma_{LEFT}$  into an empty computational domain. Its inlet velocity is  $[v_{d,x,0}, v_{d,y,0}] = [3.0, 0.0]$  m/s. It can be observed in the figure that the ice interfaces at different times move diagonally upward from the airfoil (the ice interface time is 0 s) toward the incoming droplet flow. The last ice interface in the figure is drawn at the interface time step of 120 s. The upper surface of the cable is more exposed to icing than its lower counterpart.

#### 2) Drag formulation based analysis

Case CD1 is shown in Fig. 12. In this case, droplet flow is horizontally emitted at boundary  $\Gamma_{LEFT}$  into a computational domain, filled with quiescent air. The flow velocity at the inlet is  $[v_{d,x,0}, v_{d,y,0}] = [3.0, 0.0]$  m/s. It can be observed in the figure that ice accretes more horizontally as in Case CD01. This is due to the fact that the flowing droplets experience larger resistance in the vertical direction (still air) than in Case CD01 (no air).

## V. CONCLUSIONS

A simple Lagrangian icing procedure is developed based on

a 'two fluid' multiphase model with droplets and air. After a wetted surface of PNES is determined, dry ice accretion with ice interface evolution can be computed. The study entails various cases of ice formation resembling motion of sub/supercooled droplets influenced by air and their freezing and accreting after their impact on the wind turbine blade or cable.

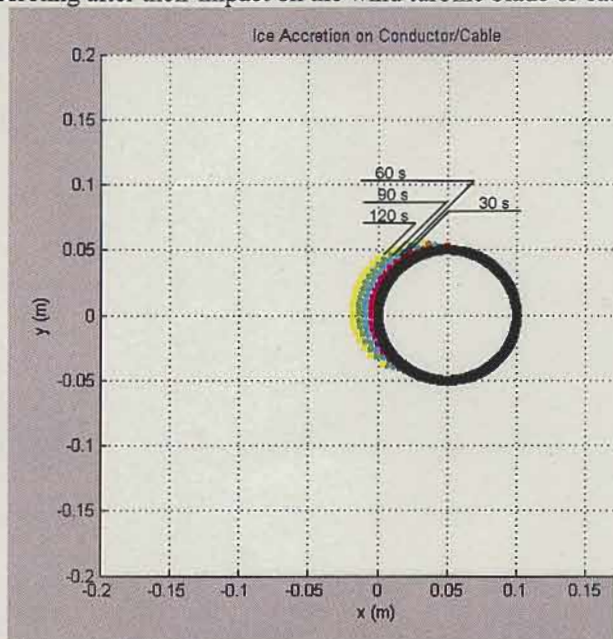


Fig. 11. Case CD01 (ice interface time step is 30 s).

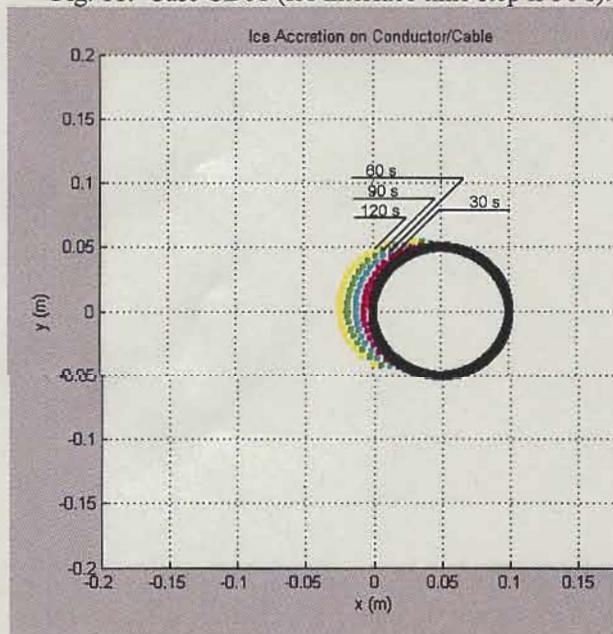


Fig. 12. Case CD1 (ice interface time step is 30 s).

Air can significantly alter motion of droplets and therefore their impact on PNES. The study involves application of interfacial drag (none, weak and strong) and its influence on the ice accretion process. The study shows that the larger the droplet phase fraction is, the faster the ice deposition on PNES will be. Shape of an ice interface is a function of flow configuration and geometry of impacted structure. Presented ice interface solutions allow calculation of ice area and ice mass. These parameters, which are controlled by the flows, the

phase fraction and the geometry are important in further studies, such as minimization of reduced aerodynamic performances of iced PNES. The study is viewed to be a useful comparative, serial and parallel companion to the models with larger applicability, involving rotational and multi-dimensional icing of wind turbine blades. Using such tools is inevitable in basic parametric studies, such as for the understanding and further description of transport properties in sub/supercooled icing conditions.

## VI. ACKNOWLEDGMENT

This work was carried out within the framework of the NSERC/Hydro-Quebec/UQAC Industrial Chair on Atmospheric Icing of Power Network Equipment (CIGELE) and the Canada Research Chair on Engineering of Power Network Atmospheric Icing (INGIVRE) at Université du Québec à Chicoutimi. The authors would like to thank the CIGELE partners (Hydro-Québec, Hydro One, Électricité de France, Alcan Cable, K-Line Insulators, CQRDA and FUQAC) whose financial support made this research possible.

## VII. REFERENCES

- [1] S. A. Slater, J. B. Young, "The calculation of inertial particle transport in dilute gas-particle flows," *Int. J. Multiphase Flow*, vol. 27, pp. 61-87, 2001.
- [2] Y. Bourgault, W. G. Habashi, J. Dompierre and G. S. Baruzzi, "A finite element method study of Eulerian droplets impingements models," *Int. J. Num. Meth. In Fluids*, vol. 29, pp. 429-449, 1999.
- [3] M. Milanez, G. F. Naterer, G. Venn, G. Richardson, "Eulerian formulation for droplet tracking in dispersed phase of turbulent multiphase flow," in *2002 AIAA 32<sup>nd</sup> Fluid Dynamic Conf., AIAA Paper 2002-3182*.
- [4] J. R. Valentine, "Application of a Lagrangian Particle Tracking Scheme in a Body-Fitted Coordinate System," *Numerical Methods in Multiphase Flows*, ASME-FED 185, pp. 39-46, 1994.
- [5] M. B. Bragg, A. P. Broeren, L. A. Blumenthal, "Iced-airfoil aerodynamics," *Progress in aerospace sci.*, vol. 41, pp. 323-362, 2005.
- [6] W. J. Jasinski, S. C. Noe, M. S. Selling, M. B. Bragg, "Wind turbine performance under icing conditions," in *1997 AIAA Meeting Papers on Disc., A9715950, AIAA Paper 97-0977*.
- [7] W. J. Jasinski, S. C. Noe, M. S. Selling, M. B. Bragg, "Wind turbine performance under icing conditions," *Journal of Solar Energy Engineering*, vol. 120, pp. 60-65, 1998.
- [8] K. J. Finstad, L. Makkonen, "Turbine blade icing model," in *1992 Proceeding International Expert's meeting on Wind Power In Icing Conditions, BOREASI*.
- [9] K. J. Finstad, L. Makkonen, "Improved numerical model for turbine icing," in *1996 Proceeding 7<sup>th</sup> International Workshops on Atmospheric icing of structures, IWAIS*.
- [10] L. Makkonen, T. Laakso, M. Marjanjemi, K. J. Finstad, "Modelling and prevention of ice accretion on wind turbines," *Wind Engineering*, vol. 25(1), pp. 3-21, 2001.
- [11] E. J. Goodwin, J. D. Mozer, A. M. Di-Gioia, B. A. Power, "Predicting ice and snow loads for transmission lines," in *1983 Proceeding 1st International Workshops on Atmospheric icing of structures, IWAIS*.
- [12] M. Farzaneh, "Ice accretion on high voltage conductors and insulators and related phenomena," *Philosoph. Trans.*, no. 358, pp. 1-35, 2000.
- [13] M. Farzaneh, "Ice accretion on energized line insulators," *International Journal of Offshore and Polar Engineering*, vol. 3, 1992.
- [14] L. Makkonen, "Modeling of Ice Accretion on Wires," *J. Climate Applied Meteor.*, vol. 23, pp. 929-939, 1984.
- [15] L. Makkonen, "Heat transfer and icing of rough cylinder," *Cold Regions Res. Technology*, vol. 10, pp. 105-116, 1985.
- [16] S. A. Morsi and A. J. Alexander, "An investigation of particle trajectories in two-phase flow systems," *J. Fluid Mech.*, vol. 55 (2), pp. 193-208, Sept. 1972.